Biosensors and Bioelectronics 215 (2022) 114564

Contents lists available at ScienceDirect

Biosensors and Bioelectronics

journal homepage: www.elsevier.com/locate/bios

An electrochemical biosensor based on electroactive peptide nanoprobes for the sensitive analysis of tumor cells

Yujing Zeng [a], Xinyu Qu [a], Beibei Nie [a], Zheying Mu [a], Chao Li [b,**], Genxi Li [a,c,*]

[a] State Key Laboratory of Analytical Chemistry for Life Science, School of Life Sciences, Nanjing University, Nanjing, 210023, PR China
[b] School of Food and Biological Engineering, Hefei University of Technology, Hefei, 230009, PR China
[c] Center for Molecular Recognition and Biosensing, School of Life Sciences, Shanghai University, Shanghai, 200444, PR China

ARTICLE INFO

Keywords:
Tumor cell analysis
Peptide nanoprobes
Noncovalent interaction
Electrochemical detection

ABSTRACT

Peptides possess many appealing and desirable features, which have attracted increasing attention in the field of electrochemical biosensing. However, peptides hardly produce noticeable electronic signals in response to target binding events. In this work, amphipathic peptides FFFGGGGRGDS with both target recognition and self-assembly capabilities are designed to be co-assembled with the electroactive species ferrocenecarboxylic acid (FcCOOH). Furthermore, the resultant electroactive peptide nanoprobes (ePNPs) are applied for sensitive electrochemical analysis of tumor cells. Specifically, tumor cells are captured by the electrode modified with the corresponding DNA aptamers, and ePNPs can then selectively bind to integrin proteins on the cell surface, thereby accompanied by a remarkable increase of electrochemical signal. Taking the assay of MDA-MB-231 cells, the fabricated biosensor can detect cancer cells with a detection limit of 7 cells mL^{-1}. Moreover, the ePNPs can act as a universal probe for the detection of different cell lines. Given the merits of easy synthesis, convenient operation, and favorable analytical performance, the proposed biosensor exhibits great potential in developing peptide-based electrochemical biosensing for clinical applications.

1. Introduction

Peptides composed of dozens of amino acids are a class of marvelous biomolecules (Frenkel-Pinter et al., 2020). To date, peptides have received substantial attention due to their unique physical and chemical properties. On the one hand, artificial peptides have the advantages of facile synthesis, chemical versatility, high stability, and excellent biocompatibility (Delfi et al., 2021; Qi et al., 2018). On the other hand, compared with other biomaterials, peptides are more diverse in the construction of higher-order structures and execution of multiple biological functions (Amit et al., 2018; Levin et al., 2020). For example, rationally designed peptides can assemble into various nanostructures such as nanospheres, linear fibers, and two-dimensional sheets, which can act as scaffolds for cargo loading via different types of noncovalent intermolecular interactions (Han et al., 2021a; Raymond and Nilsson, 2018; Zhang et al., 2020; Zhu et al., 2022). Meanwhile, peptides that mimic the behavior and function of proteins also have molecular recognition ability (Hamley, 2017). Researchers have screened many peptides that have a high affinity to specific targets. For example, Arg-Gly-Asp (RGD) tripeptide can specifically bind to integrin on the cell surface that is closely associated with tumor angiogenesis, which has been widely applied in molecular imaging and disease therapy (Fan et al., 2018; Li et al., 2021; Wang et al., 2022b; Zhang et al., 2019).

Ascribed to these appealing features, peptides have been considered as promising sensing modules for developing superior biosensors (Behi et al., 2020; Jin et al., 2022; Retout et al., 2022; Vanova et al., 2021; Wang et al., 2022c; Yuan and Liu, 2021). Particularly, peptide-based electrochemical biosensors have also been widely established in our lab for the detection of diverse analytes because of their high sensitivity, low cost, and user-friendly operation (Han et al., 2021b; Li et al., 2013, 2015, 2016; Shi et al., 2022; Sun et al., 2020; Wang et al., 2022a; Yu et al., 2016). However, typically, peptides are difficult to simultaneously achieve target recognition and signal transduction due to their poor conductivity (Joshi et al., 2022; Park et al., 2022; Xu et al., 2021). As a result, previous works are largely dependent on electroactive tag-labeled peptides (e.g., methylene blue or ferrocene), which involve time-consuming and tedious modification and purification procedures. Moreover, the cost of peptide synthesis is dramatically increased, which

* Corresponding author. State Key Laboratory of Analytical Chemistry for Life Science, School of Life Sciences, Nanjing University, Nanjing, 210023, PR China.
** Corresponding author.
E-mail addresses: lchao@hfut.edu.cn (C. Li), genxili@nju.edu.cn (G. Li).

https://doi.org/10.1016/j.bios.2022.114564
Received 28 May 2022; Received in revised form 5 July 2022; Accepted 8 July 2022
Available online 15 July 2022
0956-5663/© 2022 Elsevier B.V. All rights reserved.

is unfavorable for future large-scale applications. Also of note, since each peptide chain is generally labeled with only one electroactive tag, the sensitivity of the involved biosensors is unsatisfactory inevitably. Therefore, it has become a bottleneck to develop peptide-based electrochemical biosensors for the analysis of specific targets.

Herein, we have proposed a strategy in this work to endow peptides with electroactivity based on the design and co-assembly of amphipathic peptides and electroactive ferrocene derivatives. The fabricated biosensor has also been employed for the detection of tumor cells. Tumor cells are considered as an important type of biomarker for liquid biopsy, which possesses abundant genetic and phenotypic information (Alix-Panabières and Pantel, 2021; Keller and Pantel, 2019; Shen et al., 2017). To do so, we have rationally designed a bifunctional peptide, which can not only assemble into nanostructures and carry signal cargoes, but also recognize tumor cells with a high affinity. After tumor cells are captured by the electrode modified with corresponding DNA aptamer, the prepared electroactive peptide-based nanoprobes (ePNPs) can selectively bind to integrin that is overexpressed on certain tumor cells, which simultaneously generate remarkable electrochemical signals. Since the integrated peptide nanoprobes enable both target identification and signal transduction, tumor cells can be simply and sensitively detected.

2. Experimental section

2.1. Materials and reagents

DNA aptamer AS1411 and TLS11a were synthesized from Sangon Biotech Co. Ltd. (Shanghai, China). All peptides (≥95% purity) used in this work were chemically synthesized by the standard solid-phase method, purchased from Bankpeptide Biological Technology Co. Ltd. (Hefei, China). The sequences of oligonucleotides and peptides are listed in Table S1. Ferrocenecarboxylic acid (FcCOOH, 98% purity) was obtained from Aladdin (Shanghai, China). Pyrene was obtained from Energy Chemical (Shanghai, China). Ethylenediaminetetraacetic acid (EDTA), *N*-(2-Hydroxyethyl) piperazine-*N*′-(2-ethanesulfonic acid) (HEPES), Tris (2-carboxyethyl) phosphine hydrochloride (TCEP), and 6-Mercapto-1-hexanol (MCH) were purchased from Sigma-Aldrich (Shanghai, China). Fetal bovine serum (FBS) was obtained from Thermo Fisher Scientific, Inc. (MA, USA). Dimethyl sulfoxide (DMSO), McCoy's 5A medium, and Dulbecco's modified Eagle's medium (DMEM) were provided by Sangon Biotech Co. Ltd. (Shanghai, China). All ultrapure water used in this work was prepared by a Milli-Q system with a resistivity of 18.2 MΩ cm.

2.2. Instrumentation

Transmission electron microscopy (TEM) images and elemental mapping images were taken from JEM-2100F (JEOL Ltd., Japan). Scanning electron microscopy (SEM) images were taken from SU8020 (Hitachi Ltd., Japan). Fluorescence spectra were recorded using an FL-7000 fluorescence spectrophotometer (Hitachi Ltd., Japan). Particle sizes were measured by Zetasizer Nano ZSE (Malvern Instrument Ltd., UK) at 25 °C. All electrochemical measurements were performed with a CHI–660C electrochemical workstation (CH Instruments, Shanghai, China).

2.3. Determination of critical micelle concentration

Pyrene molecules were employed to determine the critical micelle concentration (CMC) of P1 by fluorescence spectroscopy (Klass et al., 2019). In brief, pyrene was dissolved in acetone and the acetone was then evaporated. Different concentrations of P1 solutions varying from 0.01 to 30 μM were subsequently added, keeping the final concentration of pyrene at 0.6 μM. After 30 min of sonication treatment, the solutions were kept in the dark at room temperature overnight to reach an equilibrium. The intensities of the first (λ = 373 nm) and the third (λ = 384 nm) fluorescence emission peaks of pyrene were recorded and used for CMC calculation (I_1/I_3).

2.4. Preparation of ePNPs

For the preparation of ePNPs, peptide and FcCOOH stock solutions were freshly prepared by dissolving powders in DMSO at a concentration of 1.2 mM and 120 mM, respectively. Next, 10 uL peptide solution was mixed with 10 uL FcCOOH solution, followed by sonicating for 5 min. The mixture was quickly injected into 1180 uL distilled water under stirring (Hu et al., 2017). The ePNPs precipitates were obtained by centrifugation and washed with plenty of water three times (10000 rpm, 10 min). The resulting ePNPs were suspended in 100 uL HEPES buffer (5 mM HEPES, 2.5 mM KCl, 140 mM NaCl, pH 6.8) when used for electrochemical detection.

2.5. Cell culture

MDA-MB-231, HepG2, and MCF-10A cells were cultured in DMEM medium. SKBR3 cells were cultured in McCoy's 5A medium. All media were supplemented with 10% FBS, 100 U mL^{-1} penicillin, and 100 μg mL^{-1} streptomycin. Cells were grown in a humidified atmosphere with 5% CO_2 at 37 °C, the cells were harvested and subcultured with trypsin when reached 80% confluence.

2.6. Preparation of aptamer-modified gold electrode

The gold electrode (AuE) was firstly immersed in piranha solution (H_2SO_4: H_2O_2 = 3: 1 by volume) for 30 min and then polished with 1, 0.3, 0.05 μm alumina slurry. Next, AuE was sequentially sonicated in ethanol and deionized water for 10 min. After immersing in 50% HNO_3 for another 30 min, AuE was electrochemically cleaned in 0.5 M H_2SO_4 by cyclic voltammetry (CV). The AuE was dried with nitrogen, 10 μL of aptamer immobilization buffer (10 mM Tris- HCl, 1 mM EDTA, 0.1 M NaCl, 10 mM TCEP, pH 7.4) containing 2 μM DNA aptamer was then dropped on the surface of AuE and incubated at room temperature for 2 h. Thereafter, the AuE was soaked in 1 mM MCH for 30 min to obtain ordered monolayers. After rinsing with deionized water, the prepared AuE was ready for cell capture.

2.7. Electrochemical detection of cells

The cells were collected by centrifugation at 1000 rpm for 5 min and washed with 0.01 M phosphate-buffered saline (PBS). Different concentrations of cells were obtained by diluting the higher concentration (5×10^4 cells mL^{-1}) to the desired concentration with the final volume of 1 mL. For cell analysis in complex environments, cells were spiked into 10% FBS or whole blood. The aptamer-modified AuE was then incubated with cell suspension at 37 °C for 60 min. Next, the electrode was incubated with ePNPs for another 1h at room temperature. After being rinsed with HEPES buffer, the obtained electrode was used for electrochemical detection.

For electrochemical measurements, modified AuE was employed as the working electrode, platinum wire electrode as the counter electrode, and saturated calomel electrode as the reference electrode. Electrochemical impedance spectroscopy (EIS) was conducted in 1 M KCl containing 5 mM $[Fe(CN)_6]^{3-/4-}$ with a frequency ranging from 0.1 Hz to 100 kHz. Differential pulse voltammetry (DPV) was performed from 0 to 0.6 V, with an amplitude of 0.05 V, a pulse width of 0.1 s, and a sampling width of 0.0167 s in the HEPES buffer.

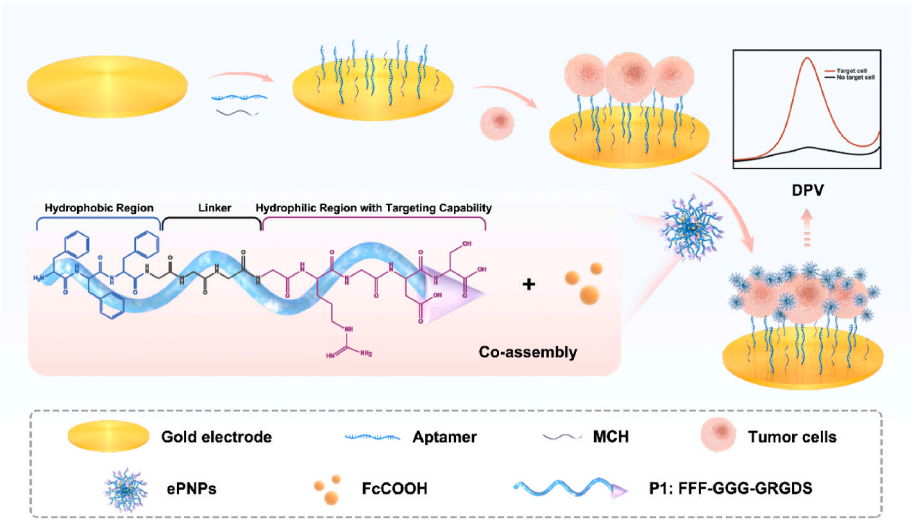

Scheme 1. Illustration of the preparation of ePNPs and electrochemical analysis of tumor cells based on ePNPs.

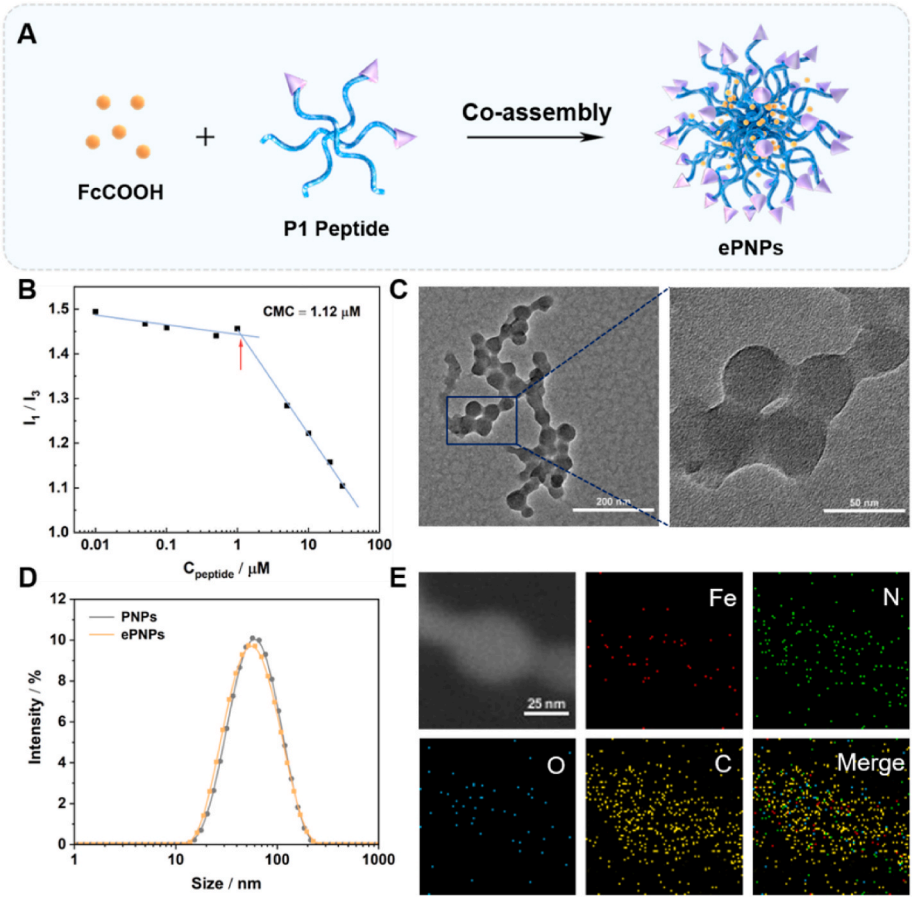

Fig. 1. Preparation and characterization of ePNPs. (A) Schematic diagram of the preparation of ePNPs. (B) Determination of the CMC of P1 (The red arrow represents the elbow point of I_1/I_3 with the change of $C_{peptide}$). *Ex* = 335 nm. (C) TEM images of ePNPs (scale bar = 200 nm). Right: a zoomed-in image of the boxed area (scale bar = 50 nm). (D) Size distribution of PNPs and ePNPs. (E) Elemental mapping images of ePNPs (scale bar = 25 nm).

3. Results and discussion

3.1. Principle of the proposed biosensor

The sensing principle of the proposed electrochemical biosensor is illustrated in Scheme 1. The designed amphiphilic peptide P1 (FFFGGGGRGDS) is composed of three regions including (1) a hydrophobic and aromatic FFF region for self-assembly, (2) a GGG flexible linker, and (3) a GRGDS region not only provides hydrophilicity but also serves as a ligand to specifically bind integrin on the cells. The ePNPs are easily prepared by quickly injecting DMSO solutions of P1 peptide and FcCOOH into water under stirring. In a typical experiment, the gold

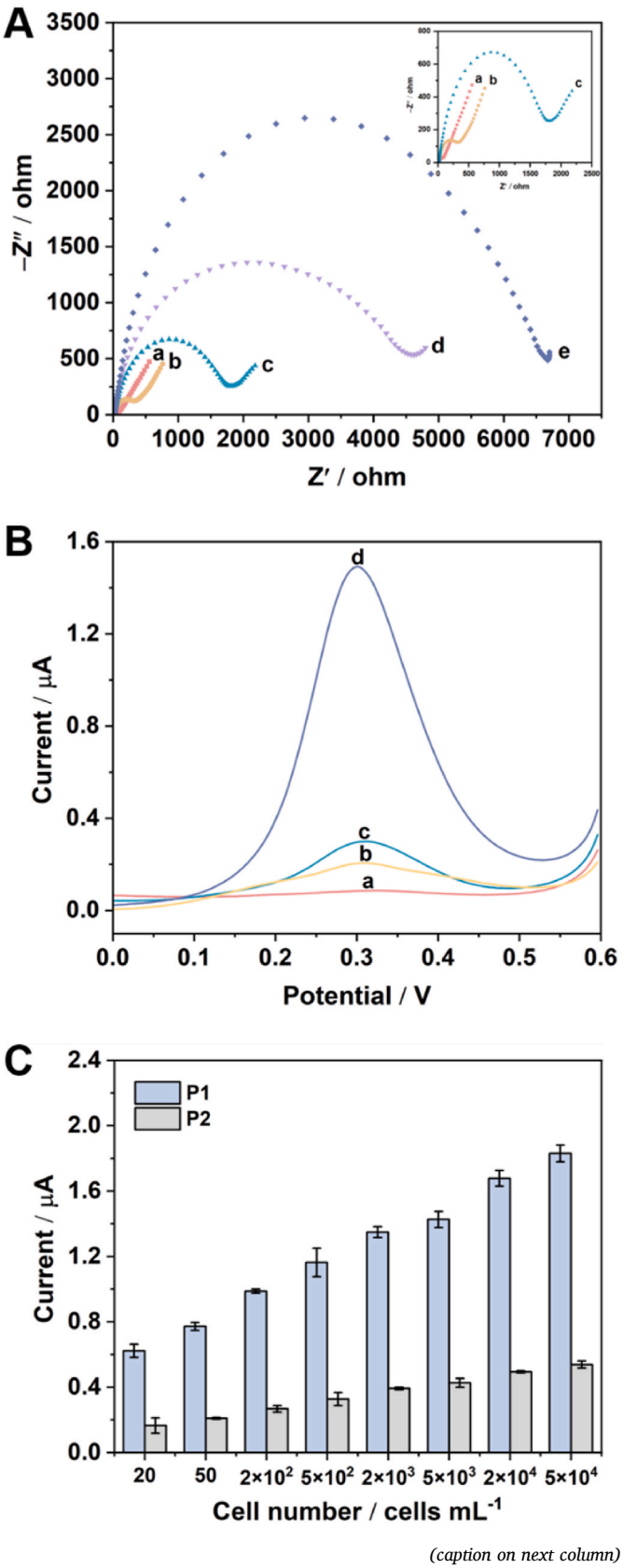

(caption on next column)

Fig. 2. The feasibility of the biosensor for tumor cell detection. (A) EIS measurements of (a) bare AuE, (b) AS1411/AuE, (c) MCH/AS1411/AuE, (d) MDA-MB-231/MCH/AS1411/AuE and (e) PNPs/MDA-MB-231/MCH/AS1411/AuE in 1 M KCl containing 5 mM $[Fe(CN)_6]^{3-/4-}$. (B) DPV responses of the electrode under different conditions. The captured cells were incubated with PNPs (curve a) or FcCOOH solution alone (curve c), incubated with ePNPs in the absence of cells (curve b) or the presence of cells (curve d). The concentration of MDA-MB-231 cells was 2×10^3 cells mL^{-1}. (C) Comparison of DPV peak currents obtained by P1 and P2 with different concentrations of MDA-MB-231 cells from 20 to 5×10^4 cells mL^{-1}. Error bars were calculated from three repeated experiments.

electrode surface is modified with DNA aptamer, which has a strong affinity to target tumor cells. Once cells are captured by the electrode, the as-prepared ePNPs are introduced and selectively bound to the integrin on the cell surface. Consequently, a distinguishable differential pulse voltammetry (DPV) signal is detected by interrogating the oxidation peak of FcCOOH.

3.2. Characterization of ePNPs

The ePNPs can be simply prepared by co-assembly of P1 peptides and electroactive molecules, FcCOOH (Fig. 1A). To evaluate the self-assembly ability of P1, so as to determine the following experimental concentration, the CMC value of P1 has first been confirmed to be about 1.12 μM by using pyrene as the fluorescent probe (Fig. 1B). The morphologies of PNPs and ePNPs have subsequently been characterized by TEM, and spherical NPs with smooth surfaces are both observed (Fig. 1C, Fig. S1). Consistent with the results of TEM, DLS analysis indicates that ePNPs have an average diameter of ~47 nm, which is slightly smaller than PNPs with an average diameter of ~55 nm (Fig. 1D). As shown in Fig. 1E, the elemental mappings of Fe, N, O, and C display a uniform distribution in ePNPs, in which the content of Fe is about 1.42 wt%. Specifically, the coexistence of Fe and N elements implies the effective incorporation of FcCOOH and peptide, respectively. The electrochemical behavior of PNPs and ePNPs has also been characterized by cyclic voltammetry (CV). Compared to PNPs, the CV curve of ePNPs shows a large pair of redox peaks, which is ascribed to the oxidation and reduction of the incorporated FcCOOH (Fig. S2). To further elucidate the possible interactions between P1 and FcCOOH, molecular docking experiments have been performed with AutoDock 4.2. The simulated hybrid structure of FcCOOH and P1 is shown in Fig. S3. The hydrophilic region (Gly 8, Arg 9, and Gly 10), and Phe 2 are the critical binding sites with FcCOOH, and the intermolecular hydrogen bonds are responsible for the binding conformation. Taken together, these results suggest the successful synthesis of ePNPs. Moreover, the interaction of ePNPs and cells has been characterized by SEM. MDA-MB-231 shows a relatively smooth cell membrane, whereas after being treated with ePNPs, spherical structures are observed to bind and aggregate on the cell surface (Fig. S4).

3.3. Feasibility of the electrochemical biosensor based on ePNPs

The electrochemical impedance spectroscopy (EIS) has first been performed using $[Fe(CN)_6]^{3-/4-}$ as a redox probe to verify the stepwise modification of the electrode. As shown in Fig. 2A, bare AuE with almost no impedance allows for rapid transfer of electrons (curve a). The electron transfer impedance (R_{et}) value gradually increases after aptamer modification (curve b) and following MCH backfilling (curve c) due to repulsion between the negatively charged DNA and $[Fe(CN)_6]^{3-/4-}$. When breast cancer cells MDA-MB-231 are effectively captured by the AS1411 aptamer, a larger R_{et} is observed, which is ascribed to the strong

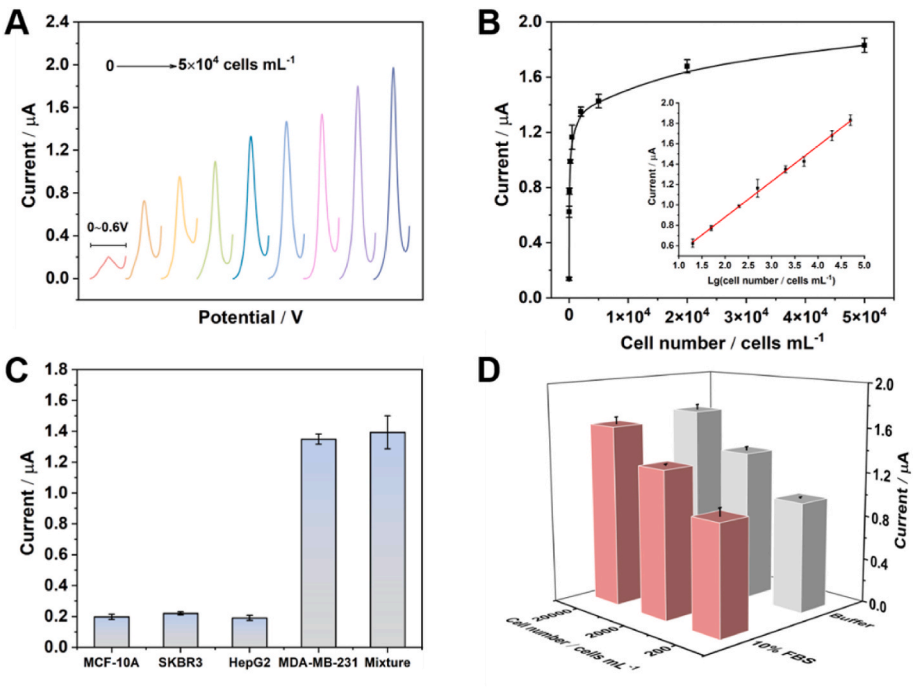

Fig. 3. Analytical performance of the proposed biosensor. (A) DPV responses of MDA-MB-231 cells at different concentrations: 0, 20, 50, 2×10^2, 5×10^2, 2×10^3, 5×10^3, 2×10^4, and 5×10^4 cells mL^{-1}. (B) The peak current values corresponding to different concentrations of cells. Inset: the linear relationship between current intensity and the logarithm of cell number. (C) The selectivity study of the proposed biosensor. Current responses to various cell types, including MCF-10A, SK-BR3, HepG2, MDA-MB-231, and the mixture of MDA-MB-231 and SKBR3. The final concentration of the cells was 2×10^3 cells mL^{-1}. (D) Comparison of current values for different concentrations of MDA-MB-231 cells in buffer and 10% FBS. Error bars were calculated from three repeated experiments.

steric hindrance of nonconductive cells (curve d). As expected, the R_{et} is conspicuously enhanced after the integration of PNPs because of the poor conductibility of the peptide, indicating the successful formation of sandwich complexes on the electrode (curve e). Meanwhile, DPV has been employed to verify the feasibility of the biosensor. As shown in Fig. 2B, only a small background current can be observed in the absence of cells (curve b), suggesting the low nonspecific adsorption of ePNPs on the electrodes. Cell-captured electrodes have also been individually incubated with PNPs, FcCOOH, and ePNPs. As a result, there is no obvious current after incubation of PNPs due to the lack of electroactive species (curve a). Besides, FcCOOH alone cannot be recruited on the cell surface, which leads to a relatively weak electrochemical signal (curve c). In contrast, a pronounced oxidation peak of Fc can be observed when ePNPs (curve d) are used.

Furthermore, we have also designed a control peptide P2 without a recognition sequence. It is not surprising that relatively weak currents are detected using P2 as the nanoprobe for all test samples with cell concentrations ranging from 20 to 5×10^4 cells mL^{-1}, which are three times lower than those using P1 (Fig. 2C). All the above results confirm the feasibility of the ePNPs-based electrochemical biosensor for tumor cell detection.

3.4. Optimization of experimental conditions

To pursue the best analytical performance, several experimental conditions have been optimized. Firstly, the impact of the aptamer on the electrochemical signals is investigated. The DPV responses quickly increase as the concentration of the aptamer increases from 0 to 2 μM but decrease at a concentration of 2.5 μM since the high density of aptamer strands may hinder the recognition of cells (Fig. S5), proving that the desired concentration is 2 μM. Then, we optimize the concentration of the ePNPs, and the DPV responses increase gradually below 10 μM and decrease thereafter. Therefore, 10 μM is chosen as the optimal concentration (Fig. S6). Finally, the incubation time between ePNPs and the cell-captured electrode is studied. As can be seen in Fig. S7, the current reaches a plateau at 60 min, thus 60 min is chosen as the reaction time for further experiments.

3.5. Analytical performance

We have utilized this biosensor for MDA-MB-231 cells capture and quantitative detection under optimal experimental conditions. Satisfyingly, the peak current of DPV increases along with the cell concentration ranging from 0 to 5×10^4 cells mL^{-1}, (Fig. 3A). There is a linear relationship between the peak current value and the logarithm of cell number (Fig. 3B). The regression equation is I (μA) = 0.3492 lgC (cells mL^{-1}) + 0.1821, with a correlation coefficient of 0.997. Additionally, the limit of detection (LOD) is calculated to be 7 cells mL^{-1} based on the 3σ rule, showing better or comparable sensitivity compared with other nanomaterials-based electrochemical methods (Table S2). The relative standard deviation (RSD) calculated from six experiments is 3.02%, suggesting acceptable reproducibility of the biosensor (Fig. S8). Moreover, the stability of ePNPs for electrochemical detection has been studied by recording the peak currents every two days under the same experimental conditions. The signals remain stable for at least 8 days, which is beneficial to its application in practical detection (Fig. S9).

Then, the selectivity of this biosensor has been explored. Significantly, the selectivity resulted from the dual recognition of functional ePNPs and AS1411 aptamer. Different cells including normal breast cell MCF-10A, breast cancer cell SKBR3, and hepatocellular carcinoma cell HepG2 are selected as the control cells. The resulting DPV responses of different cells are given in Fig. 3C, and only minor currents can be detected in controls. In contrast, obvious and similar current values can be observed from MDA-MB-231 cells and the cell mixture, demonstrating the superior selectivity of the established biosensor for target cell determination.

We have also investigated the performance of the designed biosensor in complicated samples. MDA-MB-231 cells at various concentrations have been prepared by diluting cells with 10% FBS. As shown in Fig. 3D, negligible peak current changes are observed between the buffer and 10% FBS. The biosensor has been used for cell analysis in whole blood as well. Although the peak current obtained in the blood is smaller than that in buffer or 10% FBS due to the presence of the biomacromolecule, cell debris, and residual vesicles, a significant signal enhancement is still observed compared to the control sample (Fig. S10). These results suggest that the proposed biosensor may have promising potential for clinical applications.

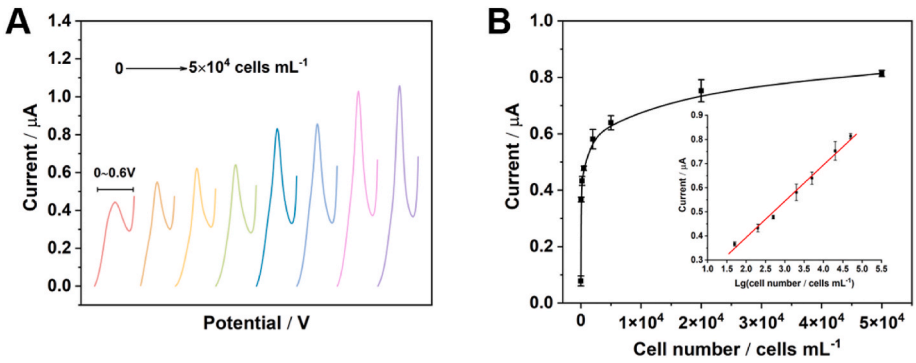

Fig. 4. Quantitative analysis of HepG2 cells using the proposed biosensor. (A) DPV responses of HepG2 cells at different concentrations: 0, 50, 2×10^2, 5×10^2, 2×10^3, 5×10^3, 2×10^4, and 5×10^4 cells mL^{-1}. (B) The peak current values corresponding to different concentrations of cells. Inset: the linear relationship between current intensity and the logarithm of cell number. Error bars were calculated from three repeated experiments.

3.6. Universality investigation of the biosensor

Since the high expression of integrin on the surface of certain tumor cells has been firmly corroborated, the proposed biosensor is allowed to detect different types of tumor cells by replacing the corresponding cell-specific aptamers. To investigate the universality of the established biosensor, ePNPs have been employed to detect HepG2 cells by changing the aptamer on the electrode to TLS11a. As shown in Fig. 4A, the DPV signal is steadily increased with increasing cell concentration, suggesting that more ePNPs are recruited to the cell surface. Fig. 4B reveals that the peak current of DPV is proportional to the logarithm of cell concentration from 50 to 5×10^4 cells mL^{-1}. The corresponding regression equation is I (μA) = 0.1502 lgC (cells mL^{-1}) + 0.0935 (R^2 = 0.986). Meanwhile, the LOD is assessed to be 13 cells mL^{-1} based on the 3σ rule. These results well-demonstrate that ePNPs can be applied as a universal electrochemical probe for tumor cell detection.

4. Conclusion

In summary, we have successfully developed an ePNP-based electrochemical biosensor for convenient and highly sensitive detection of tumor cells. Compared with conventional peptide-based electrochemical biosensors requiring chemically labeled redox reporters, the used co-assembled ePNPs via noncovalent interactions can concurrently realize molecule recognition and signal output. As a proof-of-concept test, the ePNPs have been investigated as a universal probe for different types of tumor cell detection. In addition, since the recognition motif can be substituted by different targeting sequences, our method may be adapted to other cell analysis in clinical applications.

CRediT authorship contribution statement

Yujing Zeng: Conceptualization, Methodology, Investigation, Writing – original draft. **Xinyu Qu:** Methodology, Investigation, Validation, Data curation. **Beibei Nie:** Investigation, Validation. **Zheying Mu:** Data curation, Formal analysis. **Chao Li:** Writing – review & editing, Supervision. **Genxi Li:** Writing – review & editing, Supervision, Funding acquisition.

Declaration of competing interest

The authors declare that they have no known competing financial interests or personal relationships that could have appeared to influence the work reported in this paper.

Data availability

The authors do not have permission to share data.

Acknowledgments

This work was supported by the National Natural Science Foundation of China (Grant No. 81772593), and the Fundamental Research Funds for the Central Universities (Grant Nos. 14380163 and JZ2021HGTB0120).

Appendix A. Supplementary data

Supplementary data to this article can be found online at https://doi.org/10.1016/j.bios.2022.114564.

References

Alix-Panabières, C., Pantel, K., 2021. Cancer Discov. 11, 858–873.
Amit, M., Yuran, S., Gazit, E., Reches, M., Ashkenasy, N., 2018. Adv. Mater. 30, 1707083.
Behi, M., Naficy, S., Chandrawati, R., Dehghani, F., 2020. Small 16, 1905994.
Delfi, M., Sartorius, R., Ashrafizadeh, M., Sharifi, E., Zhang, Y., De Berardinis, P., Zarrabi, A., Varma, R.S., Tay, F.R., Smith, B.R., Makvandi, P., 2021. Nano Today 38, 101119.
Fan, Z., Chang, Y., Cui, C., Sun, L., Wang, D.H., Pan, Z., Zhang, M., 2018. Nat. Commun. 9, 2605.
Frenkel-Pinter, M., Samanta, M., Ashkenasy, G., Leman, L.J., 2020. Chem. Rev. 120, 4707–4765.
Hamley, I.W., 2017. Chem. Rev. 117, 14015–14041.
Han, J., Gong, H., Ren, X., Yan, X., 2021a. Nano Today 41, 101295.
Han, Y., Zhang, Y., Wu, S., Jalalah, M., Alsareii, S.A., Yin, Y., Harraz, F.A., Li, G., 2021b. ACS Appl. Mater. Interfaces 13, 36919–36925.
Hu, X.X., He, P.P., Qi, G.B., Gao, Y.J., Lin, Y.X., Yang, C., Yang, P.P., Hao, H., Wang, L., Wang, H., 2017. ACS Nano 11, 4086–4096.
Jin, Z., Mantri, Y., Retout, M., Cheng, Y., Zhou, J., Jorns, A., Fajtova, P., Yim, W., Moore, C., Xu, M., Creyer, M.N., Borum, R.M., Zhou, J., Wu, Z., He, T., Penny, W.F., O'Donoghue, A.J., Jokerst, J.V., 2022. Angew. Chem. Int. Ed. 61, e202112995.
Joshi, P.N., Mervinetsky, E., Solomon, O., Chen, Y.-J., Yitzchaik, S., Friedler, A., 2022. Biosens. Bioelectron. 207, 114177.
Keller, L., Pantel, K., 2019. Nat. Rev. Cancer 19, 553–567.
Klass, S.H., Smith, M.J., Fiala, T.A., Lee, J.P., Omole, A.O., Han, B.-G., Downing, K.H., Kumar, S., Francis, M.B., 2019. J. Am. Chem. Soc. 141, 4291–4299.
Levin, A., Hakala, T.A., Schnaider, L., Bernardes, G.J.L., Gazit, E., Knowles, T.P.J., 2020. Nat. Rev. Chem 4, 615–634.
Li, H., Huang, Y., Yu, Y., Li, G., Karamanos, Y., 2016. ACS Appl. Mater. Interfaces 8, 2833–2839.
Li, H., Huang, Y., Yu, Y., Li, W., Yin, Y., Li, G., 2015. Anal. Chem. 87, 9251–9256.
Li, H., Wang, M., Huang, B., Zhu, S.-W., Zhou, J.-J., Chen, D.-R., Cui, R., Zhang, M., Sun, Z.-J., 2021. Nat. Commun. 12, 7149.
Li, H., Xie, H., Cao, Y., Ding, X., Yin, Y., Li, G., 2013. Anal. Chem. 85, 1047–1052.
Park, S., Park, K., Cho, H., Kwon, J., Kim, K.-s., Yang, H., 2022. Anal. Chem. 94, 4756–4762.
Qi, G.-B., Gao, Y.-J., Wang, L., Wang, H., 2018. Adv. Mater. 30, 1703444.
Raymond, D.M., Nilsson, B.L., 2018. Chem. Soc. Rev. 47, 3659–3720.
Retout, M., Mantri, Y., Jin, Z., Zhou, J., Noël, G., Donovan, B., Yim, W., Jokerst, J.V., 2022. ACS Nano 16, 6165–6175.
Shen, Z., Wu, A., Chen, X., 2017. Chem. Soc. Rev. 46, 2038–2056.
Shi, L., Kuang, D., Ma, X., Jalalah, M., Alsareii, S.A., Gao, T., Harraz, F.A., Yang, J., Li, G., 2022. Nano Lett. 22, 1083–1090.
Sun, Z., Wang, L., Wu, S., Pan, Y., Dong, Y., Zhu, S., Yang, J., Yin, Y., Li, G., 2020. Anal. Chem. 92, 3819–3826.
Vanova, V., Mitrevska, K., Milosavljevic, V., Hynek, D., Richtera, L., Adam, V., 2021. Biosens. Bioelectron. 180, 113087.

Wang, L., Li, H., Shi, L., Li, L., Jia, F., Gao, T., Li, G., 2022a. Biosens. Bioelectron. 195, 113671.
Wang, M.-D., Lv, G.-T., An, H.-W., Zhang, N.-Y., Wang, H., 2022b. Angew. Chem. Int. Ed. 61, e202113649.
Wang, M., Li, L., Zhang, L., Zhao, J., Jiang, Z., Wang, W., 2022c. Anal. Chem. 94, 431–441.
Xu, Y., Wang, X., Ding, C., Luo, X., 2021. ACS Appl. Mater. Interfaces 13, 20388–20396.
Yu, Y., Li, H., Wei, L., Li, L., Ding, Y., Li, G., 2016. Anal. Chem. 88, 3879–3884.
Yuan, L., Liu, L., 2021. Sens. Actuators, B 344, 130232.
Zhang, L., Jing, D., Jiang, N., Rojalin, T., Baehr, C.M., Zhang, D., Xiao, W., Wu, Y., Cong, Z., Li, J.J., Li, Y., Wang, L., Lam, K.S., 2020. Nat. Nanotechnol. 15, 145–153.
Zhang, X., Xi, Z., Machuki, J.O.a., Luo, J., Yang, D., Li, J., Cai, W., Yang, Y., Zhang, L., Tian, J., Guo, K., Yu, Y., Gao, F., 2019. ACS Nano 13, 5306–5325.
Zhu, X., Wang, X., Li, B., Zhang, Y., Chen, Y., Zhang, W., Wang, Y., Zhai, W., Liu, Z., Liu, S., Sun, J., Chen, Z., Gao, Y., 2022. Small 18, 2107001.